

Magnetic and transport properties of (La,Ce)Ni₂

A. Mauger

Groupe de Physique des Solides, Université de Paris VII, 2 place Jussieu, 75251 Paris CEDEX 05, France

V. Paul-Boncour, M. Escorne, A. Percheron-Guegan, and J. C. Achard

Laboratoire de Chimie Métallurgique des Terres Rares, 1 place A. Briand, 92195 Meudon Principal CEDEX, France

J. Darriet

Laboratoire de Chimie du Solide, Université de Bordeaux 1, 351 cours de la Libération, 33405 Talence CEDEX, Bordeaux, France

(Received 24 July 1989)

The magnetic and transport properties of La_{0.922}Ni₂ and Ce_{0.935}Ni₂ are investigated in the temperature range $2 \leq T \leq 250$ K. The magnetic measurements in a magnetic field $H \leq 50$ kG show an intrinsic paramagnetic behavior. They also reveal the existence of foreign magnetic impurities and of 4–6-nm nickel particles, in concentration less than 0.03%. These concentrations are so small that these defects cannot play any role in the formation of rare-earth vacancies (in concentration 5–7 at. %). An anomalous *S*-shaped rise of the resistivity has been observed, which we attribute to the existence of strong scattering of the Ni *d* conduction electrons by phonons, which dominates the spin scattering in both compounds.

I. INTRODUCTION

In previous works we have shown that both LaNi₂ and CeNi₂ crystallize with rare-earth vacancies with respect to the ideal C15-type cubic structure.^{1–3} Their true compositions are La_{1–x}Ni₂ with $x = 0.078$ and 0.097 , and Ce_{1–y}Ni₂ with $y = 0.015–0.078$.

A preliminary magnetic study of La_{0.922}Ni₂ and Ce_{0.935}Ni₂ (Ref. 3) has shown that La_{0.922}Ni₂ is a Pauli paramagnet, and that the magnetic susceptibility of Ce_{0.935}Ni₂ is almost temperature independent because of the nonmagnetic state of Ce in this compound. These results are in agreement with prior works.^{4–6} Nevertheless at low temperature, a deviation from this behavior has been observed for Ce_{0.935}Ni₂, which we attributed to the presence of Ce³⁺ ions dispersed in the matrix.

In this paper we complete this previous study, by magnetic measurements performed down to lower temperatures and up to higher magnetic fields, and by electric resistivity measurements, on the same samples as in Ref. 3. The intrinsic properties are derived and discussed. In addition, isolated magnetic impurities and Ni precipitates of a few nanometers are found in both materials. Their concentrations are deduced from the magnetic measurements and found to be several orders of magnitude smaller than rare-earth vacancies.

II. EXPERIMENTAL

The preparation and characterization of the samples are reported in Refs. 1 and 3. The samples were cut from the ingot to obtain a parallelepipedic shape: $1 \times 2 \times 5$ mm³.

The magnetization measurements in a field $H \leq 50$ kG were performed in the Laboratoire de Chimie du Solide, Bordeaux, with a superconducting quantum interference device (SQUID) magnetometer. The temperature range

investigated is $1.86 \leq T \leq 250$ K.

The sample resistance was measured by a comparator bridge method described in Ref. 7 in the range $2 \leq T \leq 300$ K. The current and potential leads were spot welded to the specimen with 0.2-mm-diam gold wires. The current contacts between the wires and the sample were small indium drops.

III. RESULTS AND DISCUSSION

A. Magnetic properties

1. La_{0.922}Ni₂

A typical low-temperature magnetization curve $M(H)$ is illustrated in Fig. 1. A hysteresis cycle is observed that vanishes at a temperature $T_f = 15$ K (Fig. 2). This hysteresis is associated with a remanent magnetization, evidenced by the difference between the field-cooled and zero-field-cooled magnetization at small magnetic fields H (see Fig. 2).

A sharp increase of the magnetization M is observed as a function of H at low fields (a few kG). Above T_f , this sharp increase is followed by a linear increase of M versus H up to the highest fields investigated, as is illustrated in Fig. 3. Below T_f , however, a non-negligible curvature of the $M(H)$ curve is observed up to the highest fields (Fig. 1). The sharp increase of M versus H at low fields above T_f suggests a Langevin-type contribution of isolated magnetic clusters in a superparamagnetic state. Since the lanthanum is not magnetic, these magnetic clusters are most likely Ni microprecipitates. If the magnetic moment μ of the clusters is assumed to be the same for all the clusters (which amounts to assuming that all the Ni particles have the same size), then the total magnetization of the material can be written

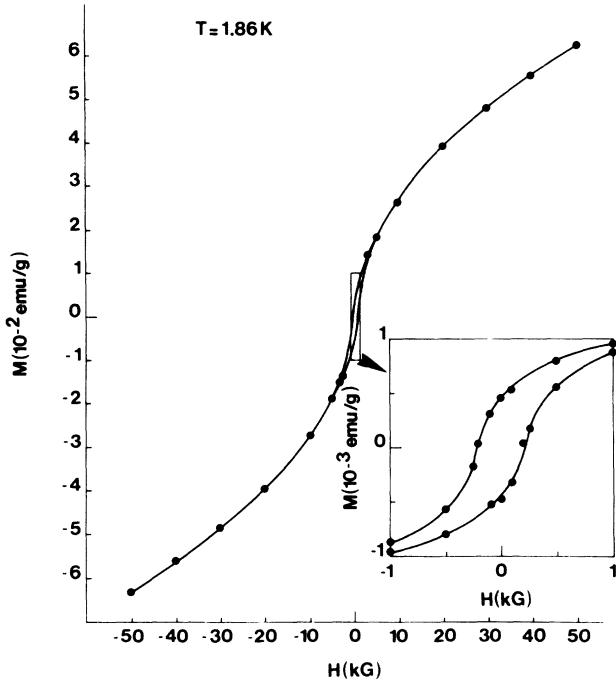


FIG. 1. Magnetization curve of $\text{La}_{0.922}\text{Ni}_2$ at $T=1.86$ K. The opening of the hysteresis cycle below the spin freezing temperature is best evidenced in the inset.

$$M = N\mu L \left[\frac{\mu H}{k_B T} \right] + \chi_P H + M_{\text{im}}. \quad (1)$$

The first term is the contribution of the Ni particles in concentration N ; L is the Langevin function. The second term in Eq. (1) represents the contribution of the conduction electrons, with χ_P the Pauli susceptibility. Since the compounds are metallic, the Fermi energy is very large, compared with the magnetic energy $\mu_B H$. It follows that

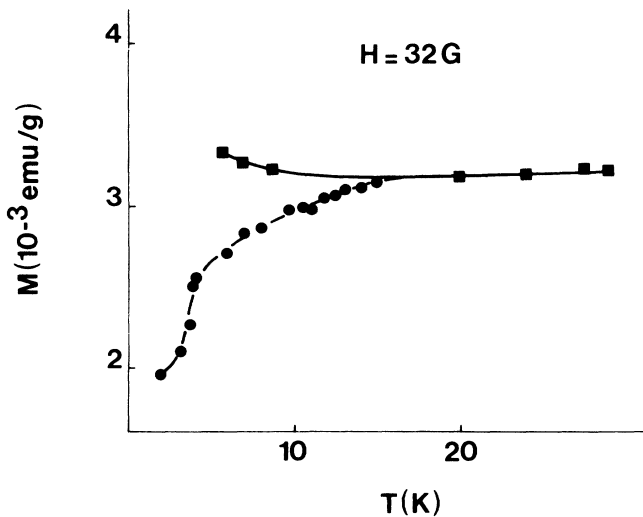


FIG. 2. Zero-field-cooled (dashed curve, ●) and field-cooled (solid curve, ■) magnetization in field $H=32$ G, measured for $\text{La}_{0.922}\text{Ni}_2$.

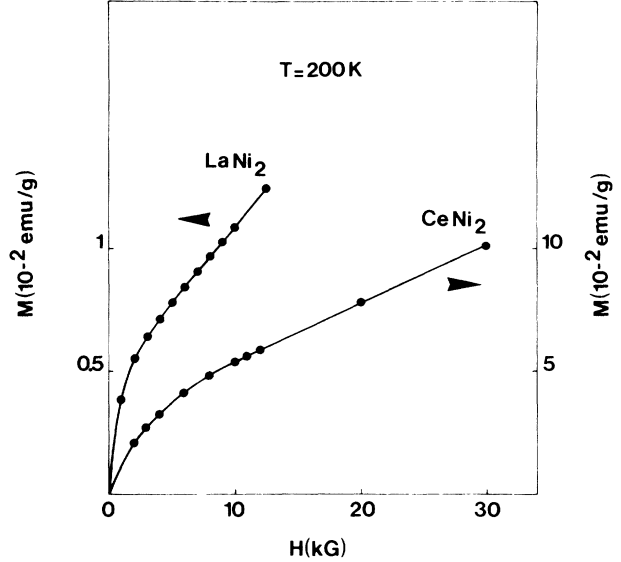


FIG. 3. Magnetization curves of $\text{La}_{0.922}\text{Ni}_2$ and $\text{Ce}_{0.935}\text{Ni}_2$, at $T=200$ K. The solid curves are theoretical fits according to the model reported in the text.

the fields available in our experiments are small enough to produce a quasilinear change in the occupation numbers $n_{\uparrow}, n_{\downarrow}$ of conduction electron states, so that the low-field linear limit $\chi_P H$ is achieved at 50 kG. The last term M_{im} in Eq. (1) is the contribution from residual magnetic impurities. For a clearer presentation of the analysis, it proves useful to make a distinction between various ranges of temperature.

(a) $100 \leq T \leq 250$ K. At such high temperatures $M_{\text{im}} \approx 0$. It is then possible to fit the experimental data $M(H)$ according to Eq. (1) with the second member reduced to the two first terms only, which still involves the three fitting parameters N , μ , and χ_P . To determine these parameters, we note the linear behavior of M versus H at high fields (see Fig. 3) arises from the $\chi_P H$ contribution, μ being large enough so that the Langevin function is close to unity. The slope of $M(H)$ at such high fields gives a good estimation of χ_P . N and μ are then determined from the low-field region $0 < H \leq 5$ kG, where the Langevin function depends significantly on H . A quantitative agreement with experiment is achieved, for temperature-independent parameters:

$$\begin{aligned} \chi_P &= 5.2 \times 10^{-7} \text{ emu/g}, \\ \mu &= 7.7 \times 10^{-17} \text{ erg/G}, \quad N = 3 \times 10^{14} \text{ g}^{-1}. \end{aligned} \quad (2)$$

Such a fit is illustrated in Fig. 3 at 200 K.

The value of χ_P is lower than the value $\chi_P \approx 3 \times 10^{-6}$ emu/g published in Ref. 3. This difference is explained by the fact that dM/dH was deduced from measurements of $M(H)$ at low fields, in which case not only is dM/dH altered by the Langevin contribution (not taken into account in Ref. 3), but also the small signal $M(H)$ is the order of the detection threshold for the vibrating sample magnetometer used in this prior work. Since the magnet-

ic moment per Ni atom in pure nickel metal is $\mu_0 = 5.36 \times 10^{-21}$ erg/G, the moment μ corresponds to Ni clusters made of $n = 1.4 \times 10^4$ Ni atoms. Their typical size s can be estimated through the relation

$$\frac{4}{3}\pi \left(\frac{s}{2} \right)^3 = \frac{a^3}{4} n,$$

with $a = 0.352$ nm, the lattice parameter for nickel. The result is $s = 6.6$ nm. The concentration N in Eq. (2) is reported per gram of the material so the fraction of Ni atoms that have precipitated to form the small Ni clusters in the material is only 2.7×10^{-4} .

(b) $T < 100$ K. Upon cooling below 100 K, a slight increase of the slope of the magnetization curve at high field is observed (Fig. 4). This effect is due to the onset of a significant contribution M_{im} of loose spins associated with residual impurities.

The criterion for the low-field limit is the same for the loose spin and the conduction-electron spin (Pauli) susceptibilities, i.e., $\mu_B H / k_B T \ll 1$, which condition is satisfied in the whole range of magnetic fields investigated for temperatures available in the experiments ($T > 1.86$ K). Therefore the H and T dependence of M_{im} is given by the Curie law:

$$M_{\text{im}} = (C_{\text{im}}/T)H, \quad (3)$$

with

$$C_{\text{im}} = N_{\text{im}} S_{\text{im}} (S_{\text{im}} + 1) g_{\text{im}}^2 \mu_B^2 / 3k_B$$

the Curie constant, provided the molecular-field approximation (MFA) is valid. Above T_f , the nonlinear magnetization at fields $H > 10$ kG is small (at most a few percent of the linear part) so that Eqs. (1) and (3) are good approximations. It is then possible to estimate the concentration of impurities N_{im} from the contribution C_{im}/T to the susceptibility $\chi = dM/dH$, at fields $H \geq 30$ kG, where the contribution from the magnetic clusters to χ is negligible.

A quantitative agreement with the data in Fig. 4 is achieved with $C_{\text{im}} = 9.17 \times 10^{-4}$ emu K/mole. We note

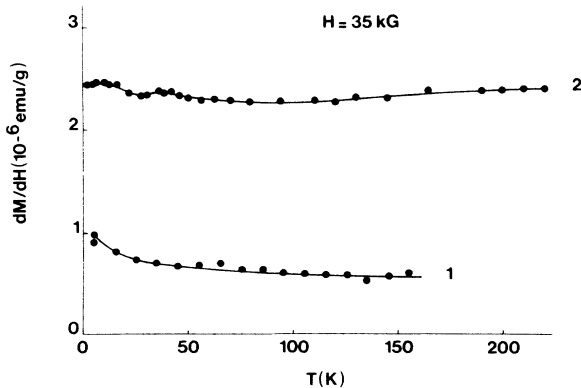


FIG. 4. In field magnetic susceptibility dM/dH measured at $H = 35$ kG, for $\text{La}_{0.922}\text{Ni}_2$ (curve 1) and $\text{Ce}_{0.935}\text{Ni}_2$ (curve 2). The uncertainty in the data is 3×10^{-8} emu/g, i.e., the order of magnitude of the radius of the dots in the figure.

this value of C_{im} is in agreement with the value expected from the existence of the magnetic impurities (mainly Pr^{3+} and Ce^{3+}) in concentrations 0.02 at. % in the metallic lanthanum. Below T_f the nonlinear magnetization becomes large (see Fig. 1). In this case the analysis of the magnetization in terms of Eqs. (1) and (3) becomes meaningless. The onset of the magnetic irreversibilities at $T_f \approx 15$ K is characteristic of a spin freezing.

The question then arises whether T_f is a temperature of transition to a spin-glass phase, or the blocking temperature of uncorrelated Ni clusters in the presence of a magnetic anisotropy. It was not possible, with our experimental set up, to investigate any critical behavior of the magnetic properties in the close vicinity of T_f , which would provide an answer to this question. We note, however, that a cusp in the high-field susceptibility curve in Fig. 4 is observed at T_f . Moreover, a blocking of the magnetic clusters can only induce a positive contribution to the slope of dM/dH at high magnetic fields, with respect to the paramagnetic regime where this contribution is negligible. The reduction of the slope dM/dH with respect to the mean-field value, upon cooling below T_f , is thus evidence of the freezing of impurity spins. We thus conclude that T_f characterizes a spin-glass-like freezing of the impurity spins at least, and possibly of the spins associated to magnetic clusters, too.

2. $\text{Ce}_{0.935}\text{Ni}_2$

The magnetic properties of $\text{Ce}_{0.935}\text{Ni}_2$ show the same features as those of $\text{La}_{0.922}\text{Ni}_2$. In particular, a hysteresis cycle is observed at low temperature (see Fig. 5). At high temperature, the sharp increase of the magnetization as a function of H , at low fields $H \leq 5$ kG, is followed by a

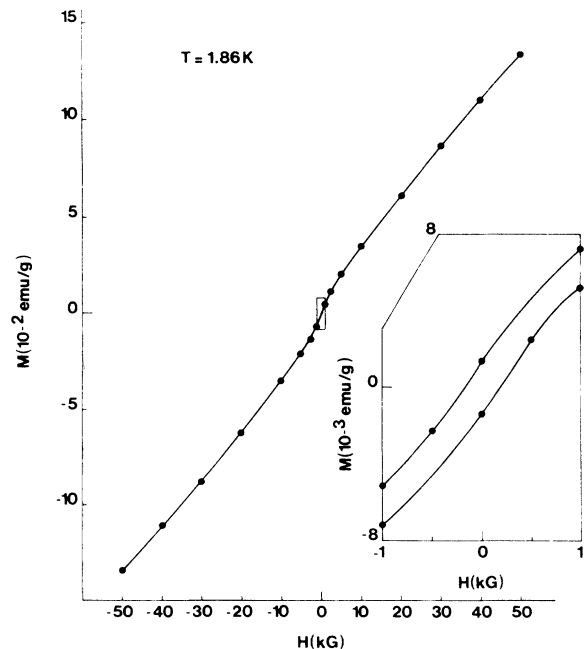


FIG. 5. Magnetization curve of $\text{Ce}_{0.935}\text{Ni}_2$ at $T = 1.86$ K; the opening of the hysteresis cycle is shown in the inset.

linear increase of M versus H at higher fields (see Fig. 3).

The magnetization can be written under the form

$$M = N\mu L \left[\frac{\mu H}{k_B T} \right] + (\chi_P + \chi_f)H + M_{\text{im}}, \quad (4)$$

which is the trivial extension of Eq. (1) modified to take into account that the total electronic magnetic susceptibility, χ_e is now the addition of the conduction (Pauli) susceptibility χ_P and the f electron susceptibility χ_f .⁸ Like in $\text{La}_{0.922}\text{Ni}_2$, χ_e is well approximated for $T > 100$ K, by the slope of the magnetization curve dM/dH measured at high field and reported in Fig. 4.

The same analysis of the magnetization curves at low fields $H < 10$ kG and $T = 200$ K, reported for $\text{La}_{0.922}\text{Ni}_2$ in the preceding paragraph allowed us to determine the fitting parameters N and μ in Eq. (4). A quantitative agreement with the magnetization curves at all temperatures $T > 100$ K is achieved for

$$\mu = 2.2 \times 10^{-17} \text{ erg/G}, \quad N = 1.28 \times 10^{14} \text{ g}^{-1}. \quad (5)$$

These values compare well with the values of these parameters in $\text{La}_{0.922}\text{Ni}_2$, so that the magnetic clusters should have the same origin in both materials, namely nickel particles. According to Eq. (5), such particles are in concentration as small as 0.03% and their typical size is 4.4 nm. The data in Fig. 4 suggest that χ_e is constant at low temperatures, a common feature in many mixed-valence materials.⁹ A small increase of dM/dH at high fields is observed upon cooling below 100 K, which can be attributed to magnetic impurities present in the cerium metal. Assuming that $\chi_e(T) \equiv \chi_e(0)$ and that Eq. (4) is satisfied, a quantitative fit of the data in Fig. 4 is achieved in the whole range $T_f < T < 100$ K, with:

$$\begin{aligned} \chi_e(0) &= 2.16 \times 10^{-6} \text{ emu/g}, \\ C_{\text{im}} &= 2 \times 10^{-3} \text{ emu K/mole}. \end{aligned} \quad (6)$$

The impurity spin freezing is evidenced by the cusp in the dM/dH curve in Fig. 4 at $T_f \approx 30$ K. Like in spin glasses, the application of a magnetic field smears out the magnetic susceptibility cusp. This is best evidenced by the reduction in amplitude of the cusp observed in Fig. 4, with respect to the cusp of the low-field magnetic susceptibility curve observed in Ref. 3.

Let us discuss the intrinsic properties. The magnetization remains small at all temperatures, which shows that the cerium is in a mixed-valence state.

Spectroscopic measurements^{10,11} suggest a Ce valence 3.2 ± 0.05 . Since, however, the valence of Ce ions as deduced from such measurements always saturates to 3.35–3.40, a value 3.2 suggests a strong mixed-valence state.

Above 100 K, Fig. 4 shows that χ_e is an increasing function of T , in agreement with previous experiments⁶ according to which χ_e goes through a maximum at $T_{\text{max}} \approx 500$ K. A scaling law for the ratio $T_{\text{max}}:C/\chi_e(0)$ has been observed for the whole class of cerium mixed-valence compounds,⁹ namely the same ratio [roughly $T_{\text{max}}:C/\chi_e(0) = \frac{1}{3}:1$] is approximately observed in CeSn_3 ,^{12,13} $\text{Ce}_{1-x}\text{La}_x\text{Be}_{13}$,¹⁴ CeN ,¹⁵ and CePd_3 ,¹⁶ with

$C = 0.807$ emu K/mole, the free Ce^{3+} ion Curie constant. According to Eq. (5), we find, for the inverse ground-state susceptibility,

$$\frac{C}{\chi_e} = 1427 \pm 10 \text{ K} \quad (7)$$

in $\text{Ce}_{0.935}\text{Ni}_2$. It follows that the above-mentioned scaling law also holds for this compound. This observation, however, only shows that this material is a standard mixed-valence system and does allow for a measurement of the valence mixing. On the other hand, such a qualitative measurement is provided by the magnitude of C/χ_e , and the value [Eq. (7)] found for $\text{Ce}_{0.935}\text{Ni}_2$ is intermediate between the values 372 and 474 K observed in almost trivalent compounds CeBe_{13} (Ref. 14) and CeSn_3 (Refs. 12 and 13), respectively, and the value 2956 K met in strongly mixed-valent CeN .¹⁵ Equation (7) is also consistent with the fact that $\chi_e(T)$ is essentially constant below 100 K, since the limit $T \ll C/\chi_e(0)$ has been reached at such temperatures.

Let us now analyze impurity effects. The magnetization data reported in this work are in quantitative agreement with our previous measurements in Ref. 3 for this sample. The analysis, however, is different. In Ref. 3, it implicitly assumed a linear dependence of M versus H for the magnetic fields investigated. The explicit measurements of M versus H in the present work clearly show that this assumption is not justified and give evidence of a Langevin-type contribution of magnetic clusters easily saturated in magnetic fields. In particular dM/dH ($H \rightarrow 0$) is dominated by this Langevin-type contribution that in the low-field limit, reduces to the Curie law with an effective Curie constant $N\mu^2/3k_B$. The confusion between this Curie constant and C_{im} led to an overestimation of the impurity concentrations in Ref. 3. Actually C_{im} compares very well with the value we have determined in $\text{La}_{0.922}\text{Ni}_2$ and presumably has the same origin, i.e., extrinsic impurities.

The value of C_{im} in Eq. (6) implies that the magnetic impurity concentration ($\leq 0.03\%$) is smaller than the vacancy concentration by 2 orders of magnitude. Therefore, Ce vacancies do not favor the formation of Ce^{3+} impurities. This is a remarkable difference with other mixed-valence systems like $\text{Sm}_{1-x}\text{V}_x\text{B}_6$,¹⁷ for example, where V also stands for rare-earth vacancies and favors the formation of Sm^{3+} .

B. Transport properties

The resistivity curves $\rho(T)$ for $\text{La}_{0.922}\text{Ni}_2$ and $\text{Ce}_{0.935}\text{Ni}_2$ are reported in Figs. 6 and 7. At $T = 0$, the residual resistivity $\rho(0)$ of $\text{La}_{0.922}\text{Ni}_2$ is larger than that of CeNi_2 , although they both are in the range $10^{-5} - 10^{-4}$ Ω cm. This is in agreement with the data reported in Ref. 18 for $\text{Ce}_{1-x}\text{La}_x\text{Ni}_2$ (if one extrapolates to $x = 1$ the data reported for $0 < x < 0.96$ in this prior work). The data for the sample referred as LaNi_2 in Ref. 18 (although the stoichiometry is unknown) make possible a more quantitative comparison with our own data for $\text{La}_{0.922}\text{Ni}_2$. The value of the residual resistivity is larger in our sample

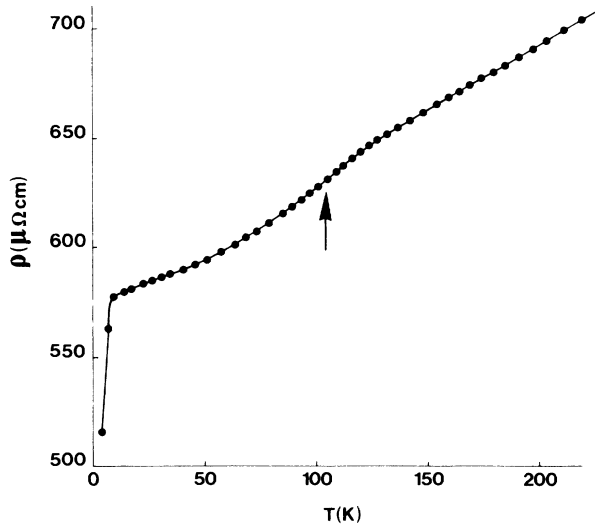


FIG. 6. Resistivity of La_{0.922}Ni₂ as a function of temperature. The arrow indicates the inflection point.

[$\rho(0)=85 \mu\Omega \text{ cm}$] than in the LaNi₂ sample of Ref. 18 [$\rho(0)=22 \mu\Omega \text{ cm}$]. This $\rho(0)$ term originates from residual impurities, local defects, dislocation lines, etc., the concentrations of which are unknown both in the sample of Ref. 18 and in our own sample (except the concentration of rare-earth vacancies in our sample, although as yet their scattering cross section is not known). As a consequence, we cannot comment on this difference in $\rho(0)$ for these two samples. In what follows, attention is focused on the variation of ρ as a function of T , which, as measured by $\rho(T)-\rho(0)$, is in good agreement with the data of Ref. 18. The $\rho(T)$ curves are *s* shaped, with an inflection point at the temperature $T_{\text{in}}=100 \text{ K}$ for La_{0.922}Ni₂ and $T_{\text{in}}=80 \text{ K}$ for Ce_{0.935}Ni₂ (see Figs. 6 and 7).

(a) La_{0.922}Ni₂. The curvature $d^2\rho/dT^2$ in the range $150 \leq T \leq 300 \text{ K}$ is very small. This result is in contrast to the saturation of the resistivity (negative $d^2\rho/dT^2$) observed and predicted when the electron mean free path becomes the order of the lattice spacing.¹⁹ We can thus conclude that, although large, the resistivity of La_{0.922}Ni₂

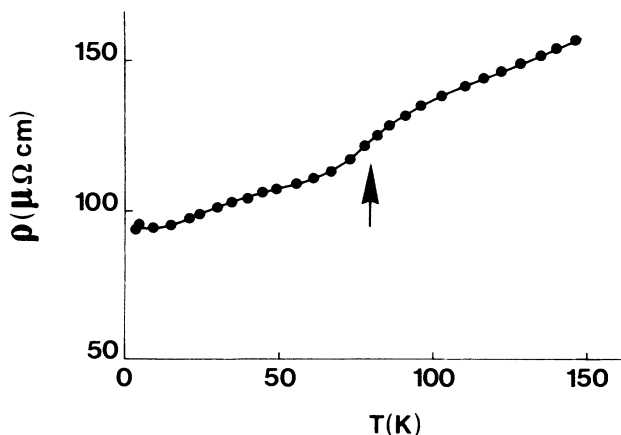


FIG. 7. Resistivity of Ce_{0.935}Ni₂ as a function of temperature. The arrow indicates the inflection point.

is still a small fraction of its maximum value below room temperature. Therefore the Matthiessen's rule applies, i.e., the various contributions to $\rho(T)$ are additive. The contribution $\rho_s(T)$ from impurity spins and Ni clusters must be temperature independent in the limit $T \gg T_f$. Since T_{in} is 1 order of magnitude larger than the spin freezing temperature T_f determined in the previous section, the Matthiessen's rule implies that the spin scattering does not play any significant role in the *s*-shaped rise of the total resistivity. We are thus led to attribute this *s* shape to an anomalous phonon scattering due to a large electron-phonon coupling. Indeed the resistivities of such lanthanide superconductors as LaAl₂ are also *s* shaped and have the same order of magnitude as La_{0.922}Ni₂, in the normal state.²⁰ The same behavior is observed in a large class of transition-metal superconductors, including the high- T_c A15 structure compounds, with T_{in} being quite generally of order 100 K.²¹ Such *s*-shaped phonon contributions to the resistivity curves can be successfully explained and attributed to a rapid dependence of the density of states at the Fermi level, resulting from a nearly empty or full high-density-of-states *d* band overlaying a low-density-of-states *s-p* band.²² This condition is fulfilled in La_{0.922}Ni₂ since spectroscopic measurements reveal that the *3d* band of nickel is nearly full.²³ We note that it is the transition element (the nickel in the occurrence) that plays the key role in the transport properties, at least above T_f . The sharp decrease of ρ upon cooling below 5 K may be a pretransitional effect in the vicinity of a superconducting critical temperature T_c . Since this effect is observed at temperatures smaller but comparable to T_f , however, it may also have the same origin as in reentrant spin glass Sn_{1-x}Mn_xTe,²⁴ i.e., a decrease of the spin scattering because of a freezing of the spin fluctuations at the scale of the mean free path of the conduction electrons.

(b) Ce_{0.935}Ni₂. The same argument as in the case of La_{0.922}Ni₂ allows us to rule out the role of the impurity and Ni cluster spin scattering in the *s*-shaped rise of $\rho(T)$ in Ce_{0.935}Ni₂. This anomaly can thus be considered as an intrinsic property. The same behavior has been observed in other Ce mixed-valence compounds.⁹ In most cases, however, the temperature scale of this transport anomaly (viz., T_{in}) is quite comparable to T_{max} deduced from the magnetic susceptibility. For example, in nearly trivalent CeSn₃ and CeBe₁₃, $T_{\text{in}}=100 \text{ K}$,²⁵ and 150 K ,²⁶ respectively, while $T_{\text{max}}=140 \text{ K}$,¹²⁻¹⁴ in strongly mixed-valence CeN, $T_{\text{in}}=600 \text{ K}$ (Ref. 27) and $T_{\text{max}}=900 \text{ K}$.¹⁵ Since T_{max} can be chosen as an order of magnitude estimate of the Ce spin fluctuation temperature, it is natural to attribute the *s*-shaped rise of the resistivity to a strong Ce-spin scattering for those compounds where $T_{\text{in}} \approx T_{\text{max}}$.⁹ In Ce_{0.935}Ni₂, however, such an interpretation does not hold, because $T_{\text{in}}=80 \text{ K}$ is very small compared to $T_{\text{max}}=500 \text{ K}$, so that the *s* shape of $\rho(T)$ in our material cannot be attributed to the scattering of the electrons by Ce-spin fluctuations.

An *s*-shaped resistivity can be, in some cases, a crystal-field effect, if T_{in} is comparable to the crystal-field splitting energy Δ of the $4f^1$ ($J=\frac{5}{2}$) ground state of the

Ce³⁺ ions.^{28,29} In mixed-valence compounds, however, the crystal-field excitation can be resolved only if the spin-fluctuation line width of the lowest multiplet (comparable to T_{\max}) is significantly smaller than Δ . Therefore, an inflection point in the $\rho(T)$ curve can be attributed to a crystal-field effect only if $T_{\text{in}} \gg T_{\max}$. When applied to Ce^{0.935}Ni₂, this argument allows us to conclude that only the inflection point of the magnetic susceptibility at $T \approx 800$ K, suggested by high-temperature measurements of Ref. 6, might be the result of crystal-field effects, but not the inflection point of $\rho(T)$ at $T_{\text{in}} \approx 80$ K.

We are thus led to conclude that the transport anomaly with $T_{\text{in}} \approx 80$ K in Ce_{0.935}Ni₂ has the same origin as in La_{0.922}Ni₂. The fact that T_{in} compares well in La_{0.922}Ni₂ and Ce_{0.935}Ni₂ also supports this conclusion. Also, the resistivity has the same order of magnitude in both materials, which suggests that the scattering of the free carriers by Ce-spin fluctuations is negligible, and supports that the dominant scattering mechanism is the diffusion of the conduction electrons by phonons. Moreover, we have already recalled that the observation of an *s*-shaped rise of $\rho(T)$ because of a strong electron-phonon scattering still requires that the Fermi level interferes with the *d* band, i.e., the transition-metal element plays a key role. This, again, is supported by the fact that, to our knowledge, intermetallics with a transition-metal element are the only cerium mixed-valence compounds that exhibit such an anomalous transport property ($T_{\text{in}} \ll T_{\max}$); another example in CeRu₂, which is most likely a very strongly mixed-valence system with a Ce-spin-fluctuation $T_{\max} > 1000$ K,⁹ while $T_{\text{in}} \approx 150$ K.²⁰

IV. CONCLUSION

The magnetic study of La_{0.922}Ni₂ and Ce_{0.935}Ni₂ shows that these compounds are a Pauli paramagnet and a Ce mixed-valence compound, respectively. It also reveals the existence of foreign magnetic impurities in concentration 0.03 at. %, and Ni small particles with typical sizes 4–6 nm and in concentration $\leq 0.03\%$. These values are 2 orders of magnitude smaller than the rare-earth vacancy concentration that is 7.8 at. % for La_{0.922}Ni₂ and 6.5 at. % for Ce_{0.935}Ni₂. The Ni concentration is so small that a uniform distribution in the bulk is unlikely. Instead, we suspect that the small particles are located near the surface, and are formed via a surface segregation mechanism as described for LaNi₅.³⁰

The transport properties have shown an anomalous *s*-shaped rise of the resistivity we attribute to the existence of a strong electron-phonon interaction. We conclude that the scattering of the *d* electrons of nickel by phonons dominates the behavior of the resistivity in La_{0.922}Ni₂ and its nonmagnetic counterpart Ce_{0.935}Ni₂. This result corroborates the suggestion that the transition metal and the electron-phonon scattering play a key role in mixed-valence cerium intermetallics.

ACKNOWLEDGMENTS

The Laboratoire de Chimie Métallurgique des Terres Rares is "Unité Propre de Recherche au Centre National de la Recherche Scientifique" No. 209; the Laboratoire de Chimie du Solide is "Laboratoire Propre au Centre National de la Recherche Scientifique" No. 8661.

- ¹V. Paul-Boncour, A. Percheron-Guegan, M. Diaf, and J. C. Achard, *J. Less-Common Met.* **131**, 201 (1987).
- ²V. Paul-Boncour, C. Lartigue, A. Percheron-Guegan, J. C. Achard, and J. Pannetier, *J. Less-Common Met.* **143**, 301 (1988).
- ³V. Paul-Boncour, A. Percheron-Guegan, M. Escorne, A. Mauger, and J. C. Achard, *Z. Phys. Chem.* (to be published).
- ⁴J. Wurcher, *J. Phys. Radium* **13**, 278 (1952).
- ⁵W. E. Wallace, T. V. Volkman, and R. S. Craig, *J. Phys. Chem. Solids* **31**, 2185 (1970).
- ⁶G. Olcese, *Solid State Commun.* **35**, 87 (1980).
- ⁷M. Escorne, Ph.D. thesis, Université de Paris, 1979.
- ⁸T. A. Costi, *J. Phys. C* **19**, 5683 (1986).
- ⁹J. M. Lawrence, P. S. Riseborough, and R. D. Parks, *Rep. Prog. Phys.* **44**, 1 (1981).
- ¹⁰K. R. Bauchspies, W. Boksh, E. Holland Moriz, H. Launois, R. Pott, and D. Wohleben, in *Valence Fluctuation in Solids* (North-Holland, Amsterdam, 1981), p. 417.
- ¹¹G. Strasser, F. V. Hillebrecht, and F. N. Netzer, *J. Phys. F* **13**, L223 (1983).
- ¹²J. Lawrence, *Phys. Rev. B* **20**, 3770 (1979).
- ¹³K. H. J. Buschow, V. Goebel, and E. Dormann, *Phys. Status Solidi B* **93**, 607 (1979).
- ¹⁴J. P. Kappler and A. Meyer, *J. Phys. F* **9**, 143 (1979).
- ¹⁵G. Olcese, *J. Phys. F* **9**, 569 (1979).
- ¹⁶W. E. Gardner, J. Penfold, T. F. Smith, and I. R. Harris, *J. Phys. F* **2**, 133 (1972).
- ¹⁷T. Kasuya, K. Kojima, and M. Kasuya, in *Valence Instabilities and Related Narrow Band Phenomena*, edited by R. D. Parks (Plenum, New York, 1977), p. 137.
- ¹⁸J. Sakurai, Y. Tagawa, and Y. Komura, *J. Magn. Magn. Mater.* **52**, 205 (1985).
- ¹⁹Z. Fisk and G. Welb, *Phys. Rev. Lett.* **36**, 1084 (1976).
- ²⁰H. J. Van Daal and K. H. J. Buschow, *Phys. Status Solidi A* **3**, 853 (1970).
- ²¹See, for example, Z. Fisk and A. C. Lawson, *Solid State Commun.* **13**, 277 (1973), and references therein.
- ²²R. W. Cohen, G. D. Cody, and J. J. Halloran, *Phys. Rev. Lett.* **19**, 840 (1967).
- ²³T. K. Hatwar and D. R. Chopra, *J. Electron Spectrosc. Relat. Phenom.* **35**, 77 (1985).
- ²⁴A. Mauger and M. Escorne, *Phys. Rev. B* **35**, 1902 (1987).
- ²⁵B. Stalinski, Z. Kletowski, and Z. Henkie, *Phys. Status Solidi A* **19**, K165 (1973).
- ²⁶G. Krill, J. P. Kappler, M. F. Ravet, A. Amamou, and A. Meyer, *J. Phys. (Paris)* **41**, 1121 (1980).
- ²⁷B. Cornut, Ph.D. thesis, Université de Grenoble, France, 1976.
- ²⁸B. Coqblin and J. R. Schrieffer, *Phys. Rev.* **185**, 847 (1969).
- ²⁹M. Escorne, A. Mauger, D. Ravot, and J. C. Achard, *J. Phys.* **14**, 1821 (1981).
- ³⁰L. Schlapbach and R. C. Brundle, *J. Phys. (Paris)* **42**, 1025 (1981).